JACS
JOURNAL OF THE AMERICAN CHEMICAL SOCIETY
Article
pubs.acs.org/JACS

Spatially Resolved Raman Spectroelectrochemistry of Solid-State Polythiophene/Viologen Memory Devices

Rajesh Kumar,[†,‡,∥] Rajesh G. Pillai,[†,‡] Nikola Pekas,[‡] Yiliang Wu,[§] and Richard L. McCreery*[,†,‡]

[†]Department of Chemistry, University of Alberta, Edmonton, Alberta, Canada
[‡]National Institute for Nanotechnology, National Research Council Canada, Edmonton, Alberta, Canada
[§]Xerox Research Centre of Canada, 2660 Speakman Drive Mississauga, Ontario, L5K 2L1, Canada

Supporting Information

ABSTRACT: A three terminal molecular memory device was monitored with in situ Raman spectroscopy during bias-induced switching between two metastable states having different conductivity. The device structure is similar to that of a polythiophene field effect transistor, but ethylviologen perchlorate was added to provide a redox counter-reaction to accompany polythiophene redox reactions. The conductivity of the polythiophene layer was reversibly switched between high and low conductance states with a "write/erase" (W/E) bias, while a separate readout circuit monitored the polymer conductance. Raman spectroscopy revealed reversible polythiophene oxidation to its polaron form accompanied by a one-electron viologen reduction. "Write", "read", and "erase" operations were repeatable, with only minor degradation of response after 200 W/E cycles. The devices exhibited switching immediately after fabrication and did not require an "electroforming" step required in many types of memory devices. Spatially resolved Raman spectroscopy revealed polaron formation throughout the polymer layer, even away from the electrodes in the channel and drain regions, indicating that thiophene oxidation "propagates" by growth of the conducting polaron form away from the source electrode. The results definitively demonstrate concurrent redox reactions of both polythiophene and viologen in solid-state devices and correlate such reactions with device conductivity. The mechanism deduced from spectroscopic and electronic monitoring should guide significant improvements in memory performance.

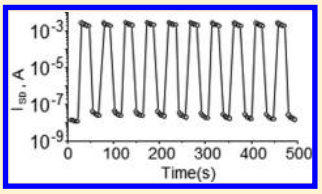

INTRODUCTION

Many resistive memory devices have been investigated as alternatives to commonly used charge storage and magnetic memory elements, in part to improve retention, power consumption, and areal density. Resistive memory is based on a material that has at least two metastable states with differing conductivity with a means to switch between the states by a "write" or "erase" (W/E) stimulus. Widely used "flash" memory is an example, based on a change in conductance of an FET structure induced by charging and discharging a floating gate of silicon isolated by SiO_2. The relatively slow W/E speed of flash, its high working voltage, and limited cycle life have stimulated a large body of work into both inorganic and organic alternatives. Of particular relevance to the current report are resistive memory devices, in which a redox reaction mediates the conductance change.[1,2] For example, a TiO_2 layer between two metallic electrodes may switch between high and low conduction states by redox reactions and oxygen vacancy migration driven by an external bias.[3] Although many examples of metal-oxide based memory devices are available, the role of ion motion and the "electroforming" process for initiating memory action are often not well understood.[1,4] Resistive memory can also be made using conducting polymers such as poly(3-hexylthiophene) (P3HT)[5−7] and polypyrrole (PPy).[6,8] Our group has reported several two-terminal memory devices based on redox activity in TiO_2 and organic molecules, including PPy.[5,6,9,10] In the case of PPy/TiO_2 heterojunctions, oxidation of PPy was established spectroscopically in response to an applied bias in the solid state, but redox activity was not directly correlated with changes in conductance.[11] Due in part to difficulties in characterizing and monitoring the operation of working microelectronic devices,[12] the mechanisms of many organic and inorganic resistive switching devices are not well established, a problem that impedes further development and wide-scale applications. The current investigation explores the switching mechanism of a polymer-based resistive memory device using Raman spectroscopy to characterize and monitor the composition and dynamics of the device during memory operation. The device structure shown in Figure 1b is similar to that of an organic field-effect transistor (O-FET), but its operation is fundamentally different. It has three electrodes, in order to separate the "write/erase" circuit from the "read" operation, and the familiar designations "source" (S), "drain" (D), and "gate" (G) will be used to distinguish the electrodes. Figure 1a shows a simpler, two-terminal structure used to diagnose the mechanism of observed conductivity changes. It resembles the electrochemically gated transistor introduced by Wrighton et al.[13] and explored for electrochemical logic devices,[14] but it uses a solid rather than liquid electrolyte. The critical component is a polymer that can be switched between insulating and conducting states by a bias-induced redox reaction. Polythiophenes [e.g., poly(3-hexylthiophene), P3HT] are extensively studied and have shown significant

Received: May 8, 2012
Published: August 2, 2012

dx.doi.org/10.1021/ja304458s | J. Am. Chem. Soc. 2012, 134, 14869−14876

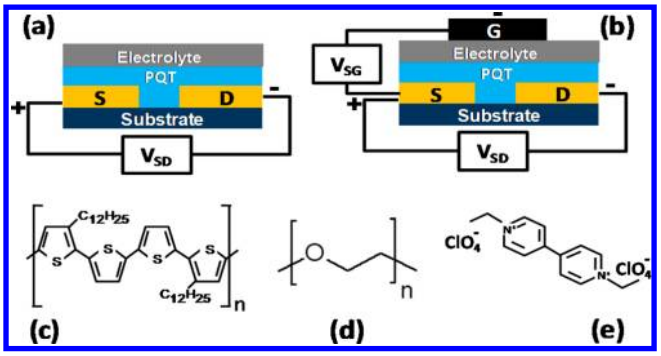

Figure 1. Schematic of experimental devices under investigation: (a) two terminal, open face and (b) three terminal with gate geometries. Chemical structures of (c) the neutral form of PQT-12, (d) PEO, and (e) ethyl viologen diperchlorate. Layer dimensions are not shown to scale.

potential in organic electronics,[15−17] including memory applications.[5−7] Upon chemical or electrochemical oxidation, a radical cation (polaron) is formed that exhibits markedly increased electronic conductivity. A thiophene-based conducting polymer similar in structure to P3HT is poly(3,3‴-didodecylquaterthiophene) (PQT), which has good electronic properties for applications in thin film transistors.[16−19] PQT is a good choice for redox-based resistive memory device due to its processability and stability under ambient conditions.[18] Other important constituents in redox-based memories are a redox-active species to support the polymer oxidation and reduction processes and a counterion to simultaneously stabilize the charged form of the polymer. Without such components, the polymer oxidation would result in a space charge that would limit oxidation and provide a strong driving force for reduction of the polaron and therefore short retention. Viologens[20,21] are reducible materials used in solid-state electrochromic devices that may undergo one- or two-electron reductions. Furthermore, viologens are available with appropriate anions (e.g., perchlorate) that can act as the counterions for polaron stabilization. Lithium perchlorate in polyethylene oxide (PEO) matrix has been used successfully as a solid electrolyte for organic electronics in general and thin film transistors in particular.[22] Ethyl viologen diperchlorate [EV-$(ClO_4)_2$] is both a good candidate for a counter-reaction to PQT oxidation and a source of mobile perchlorate ions. Thus, we expect the PQT/EV$(ClO_4)_2$ + PEO system to provide all the necessary components for a redox memory device, with the conductance between the S and D electrodes indicating the state of the PQT layer. Structures of PQT, EV$(ClO_4)_2$, and PEO are shown in Figure 1.

Spatially resolved Raman spectroscopy was used to monitor both the PQT and viologen redox processes in both the "open" two-electrode geometry (Figure 1a) and the "buried" three-electrode geometry through a partially transparent gate electrode (Figure 1b). Raman spectral changes were monitored during conductance changes to determine how redox reactions induced by SG bias pulses control SD conductance. The results reveal that a redox counter-reaction is essential to polythiophene redox-based resistive memory and permit visualization of polaron distribution throughout the device.

EXPERIMENTAL SECTION

Although the source, gate, and drain electrodes shown in Figure 1 will be referred to as S, G, and D by analogy with thin film transistors (TFT), the operation of the current devices differs fundamentally from standard organic TFTs. All the devices were made on substrates with patterned S and D electrodes of 50-nm thick Au film deposited using e-beam evaporation preceded by a 5-nm adhesion layer of Cr. The S and D terminals were patterned using standard photolithography and lift-off methods on commercially available Si/SiO_2 (300 nm) wafers. S and D electrodes are 0.5 mm wide and the channel gap is 1 μm. After the lift-off process, the substrates were ultrasonically cleaned in acetone, 2-propanol, and ultrapure water, followed by drying in a stream of nitrogen. Polyethylene oxide (PEO, MW = 100 000) and ethyl viologen diperchlorate were purchased from Sigma-Aldrich and used as received. The conducting polymer, PQT-12 (M_w = 123 000 and M_n = 32 000), was provided by the Xerox Research Centre of Canada, Ltd., as a 0.3 wt % solution in 1, 2-dichlorobenzene. PQT was spin-coated at 1000 rpm for 120 s on clean Si/SiO_2/Au chips to yield a 20−30 nm thick film. Details of the spin-coating process have been discussed elsewhere.[5] The spin-coated devices were dried and annealed in a vacuum oven (~10^{-2} Torr) at 100 °C for 1 h and then at 140−145 °C for 20 min.[17]

The electrolyte solution was prepared by mixing equal weights of 4 wt % ethyl viologen diperchlorate in acetonitrile and 5 wt % PEO in acetonitrile. The PEO solution was filtered through a 0.45 μm PTFE filter before adding the viologen solution. The electrolyte layer was deposited by drop casting 3 μL of electrolyte solution over the annealed PQT film. The devices were dried in house vacuum for ~5 min to remove residual solvent and stabilize the drop-cast film prior to insertion into the electron-beam evaporator. A few devices (<10%) were rejected due to misalignment of the electrolyte drop and the SD region. The 1 mm wide G electrode was defined by e-beam evaporation of 15 nm of carbon and 15 nm of Au through a shadow mask,[23,24] with an evaporation rate of 0.5−1 Å/s. All e-beam deposition was performed in a Kurt J. Lesker PVD-75 e-beam evaporator, which was pumped down to a base pressure of <3 × 10^{-6} Torr prior to deposition.

Current−voltage (I−V) characteristics of devices were measured using a potentiostat (CH Instruments 420A) by connecting the working electrode lead at the S terminal and both reference and counter electrode leads at either the D or G terminal in two- and three-terminal devices, as indicated in Figures 2 and 4. Memory

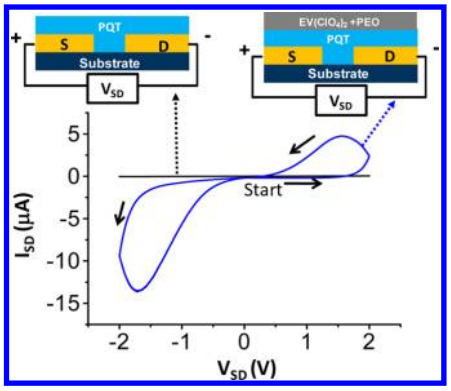

Figure 2. Two-terminal (SD) I−V sweeps for two different devices, obtained with sweep rate of 20 mV/s. Voltage on the x-axis is the S electrode relative to to D.

characteristics were measured using a National Instruments 6110DAQ board, an SRS 570 current amplifier, and LabVIEW software.[6] Repetitive W/R/E/R memory cycles were recorded with a Keithley 2602A dual channel source measure unit which permitted simultaneous control of both the SG and SD circuits. Custom test scripts were used to control the unit through a GPIB (IEEE-488) interface. The write or erase pulses were applied between the S and G terminals in the test device, and the "readout" pulses were applied between S and D while G was floating. In all cases, the applied voltage is stated as the S electrode relative to D or G; i.e., V_{SD} is the bias on the S electrode relative to D and V_{SG} is S relative to G. A Nicolet Almega XR Raman

dx.doi.org/10.1021/ja304458s | J. Am. Chem. Soc. 2012, 134, 14869−14876

microscope (Thermo Scientific) equipped with a CCD detector was employed for Raman spectroscopy and imaging with an excitation wavelength of 780 nm and 10 s integration time for each spectrum. The Raman laser was focused at the desired sample location using a 10× objective lens to yield an approximate spot size of 3 μm and power of 30 mW at the sample.

RESULTS AND DISCUSSION

The dynamics of the PQT/EV system were investigated first in the "open face" geometry (Figure 1a), in order to compare spectroscopic changes and current/voltage behavior. Raman spectra were acquired through the electrolyte and polymer layers at the positions indicated in the figures, while a bias was applied. Figure 2 shows current voltage ($I-V$) curves acquired with a 20 mV/s scan rate for two different devices in two-terminal geometry with and without a PEO/EV electrolyte layer. Structures of the two different devices are also shown next to the $I-V$ curves. A representative device containing only PQT shows a linear $I-V$ curve with very low current (<30 nA) in the voltage range of −2 to +2 V (black line). The ±2 V range was selected initially on the basis of the positions of the features in the $I-V$ curve and was expanded in subsequent testing (below). This $I-V$ curve for a PQT only device is shown with a magnified current axis as Figure S1 in the Supporting Information. The low currents for the two-terminal Au/PQT/Au devices is due to the low conductivity of the undoped PQT film between the S and D electrodes. However, the device with both PQT and PEO/EV layers (Figure 2, blue curve) shows a nonlinear $I-V$ relationship with much larger current compared to the PQT-only device. During the positive SD voltage sweep (forward cycle), an increase in SD current magnitude was observed when the S bias exceeds ∼1.5 V with respect to D. A similar increase in SD current was observed in the reverse cycle with D bias of ∼1.5 V with respect to S. In a previous two-terminal experiment using a "sandwich" geometry, we observed oxidation of polythiophene using Raman spectroscopy, but a layer of SiO_2 prevented measurement of conductance changes.[5] The results shown in Figure 2 imply that a significant conductance change has occurred when both PQT and EV/PEO are present and a bias is applied. Since the structure in Figure 2 is symmetric in terms of composition, there is a similar increase in current due to PQT oxidation when either the S or D electrode is positive. When a pristine device was scanned initially in the negative V_{SD} direction, the difference in peak heights apparent in Figure 2 is reversed, indicating that the $I-V$ response is approximately symmetric.

To probe structural changes in the two-terminal device accompanying a V_{SD} bias, Raman spectra were obtained at the D and S electrodes in order to monitor changes in PQT^0 (neutral), PQT^+ (polaron), EV^{2+}, EV^+, and EV^0 concentrations. Raman spectra under different bias conditions are shown in Figure 3. The Raman spectrum from the as-prepared device before bias was applied (Figure 3a) shows a major peak at 1460 cm^{-1} corresponding to neutral, undoped PQT. The Raman spectrum from the same position on S electrode with a V_{SD} = +2 V (Figure 3b) has a major peak at 1405 cm^{-1} corresponding to the PQT polaron. Reference spectra of undoped PQT and its chemically oxidized (using $FeCl_3$) form are provided in Figure S2 in Supporting Information. Although it is possible that both the polaron and bipolaron forms of PQT are formed in the solid-state devices, there is no direct evidence for bipolaron formation. For the opposite bias (V_{SD} = −2 V) the S is negatively biased and polarons are reduced back to the neutral form, with the major peak at 1460 cm^{-1} for reduced PQT reappearing (Figure 3c). Compared to spectrum 3a, the spectrum for V_{SD}= −2 V shows two additional bands at 1028 and 1528 cm^{-1} (marked with *). Reduction of EV^{+2} with either borohydride (Figure S3, Supporting Information) or electrochemically (Figure S4, Supporting Information) reveal Raman peaks at 1028 and 1528 cm^{-1}, which are attributable to the one-electron-reduced species, EV^+, consistent with reported peak frequencies.[20] As expected from the symmetry of the two-terminal device, monitoring the Raman spectrum above the D electrode yielded similar results, with reverse polarity (Figure S5, Supporting Information).

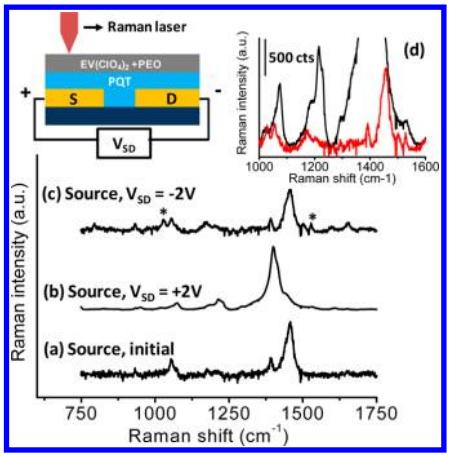

Figure 3. Raman spectra obtained at the source for the indicated V_{SD} values in the two-terminal open face geometry containing stacked layers of PQT and $EV(ClO_4)_2$ + PEO. Raman spectra show a shift in characteristic PQT peak due to formation of polaron for V_{SD} = 2 V. The Raman spectrum shows the reduced form of viologen (marked with *) when S is biased negative. The inset shows device schematic and the overlay of Raman spectra on the same scale, from the S electrode for V_{SD} = +2 V (black curve) and −2 V (red).

For two-terminal Au/PQT/Au devices lacking a EV-PEO layer, the Raman spectra from S and D electrodes did not change for any bias between +2 and −2 V (Figure S6, Supporting Information). The spectroscopic and voltammetric results are consistent with "dynamic doping" of the PQT polymer by oxidation during an applied bias. The ∼25 nm PQT layer is sufficiently thin to permit reduction of EV^{+2} to EV^+ at the negative electrode. There is likely motion of ClO_4^- into the polymer layer during PQT oxidation, although there is no direct spectroscopic evidence of such ion motion. The oxidized form of PQT persists during the reverse scan, causing the hysteresis apparent in the $I-V$ curve of Figure 2. The two-terminal geometry of Figure 1a provides a clear correlation between polymer oxidation and conductance changes, but it is not ideal for a memory device because of possible interference between the W/E process and conductance readout. The three-terminal geometry of Figure 1b provides separate circuits for W/E and readout and also enables the conductance readout along a relatively long path between S and D but W/E pulses across a shorter path between S and G.

Figure 4 shows a an $I-V$ curve for a three-terminal Au/PQT/$EV(ClO_4)_2$ + PEO/C/Au device scanned between V_{SG} = −2 and +2 V (red line). An $I-V$ curve from a PQT device without the $EV(ClO_4)_2$ layer is also shown for comparison (black curve), which is magnified as Figure S7 in the Supporting Information. Bias polarities and layer constituents are shown in the inset in Figure 4, and the arrows show the

dx.doi.org/10.1021/ja304458s | J. Am. Chem. Soc. 2012, 134, 14869−14876

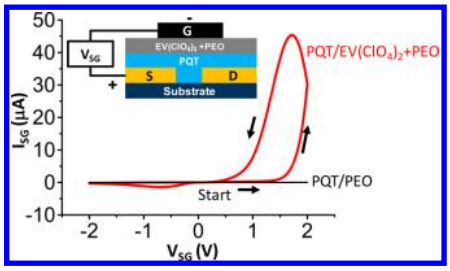

Figure 4. Source−gate I−V curve for finished device with a C(15 nm)/Au(15 nm) gate. Increase in SG current around 1.5 V is due to oxidation of PQT accompanied by ethyl viologen reduction. The same curves are plotted on a logarithmic scale in Figure S8 in the Supporting Information.

direction of sweep starting from V_{SG} = 0. An asymmetric I_{SG}−V_{SG} is apparent with more current when S is biased positive with respect to G and an asymmetry ratio of ∼100 for $|V_{SG}|$ = 2 V. When S is biased positive beyond a certain threshold (∼1.5 V in the present case), PQT is oxidized to its conducting polaron (PQT^+) and EV^{+2} is reduced to EV^+ at G. The E^o values for $PQT^{+/0}$ and $EV^{+2/+1}$ are +0.76 and −0.45 V vs NHE, so the predicted E^o_{cell} for the PQT/EV system is ∼1.21 V. This E^o is different in the solid state, since the components are not at unit activity, but it does provide an estimate of the minimum bias required to carry out the cell reaction (eq 1).

$$PQT + EV^{+2} = PQT^+ + EV^+ \quad (1)$$

Under reversed polarity with V_{SG} negative, current through the SG circuit is small because PQT is now reduced and its conductivity is low. As shown in Figure 4, devices with only PQT and PEO but lacking EV show small currents with minimal conductance change for V_{SG} = ±2 V, since there is no redox counter-reaction. Further support for the redox mechanism is provided by in situ Raman spectroscopy of the three-terminal device under different V_{SG} conditions. Figure 5 shows the Raman spectra from S and D electrodes from Au/PQT/$EV(ClO_4)_2$ + PEO/C/Au devices during various SG biases. Spectra 5a−c were acquired through the PQT and EV/

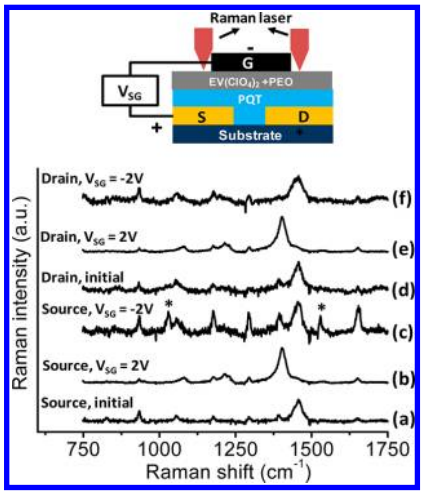

Figure 5. Effect of SG bias on Raman spectra at S and D electrodes in the Au/PQT/$EV(ClO_4)_2$ + PEO/C/Au devices. Only S sees bias, but both S and D show reversible polaron formation with appropriate SG bias. Peaks corresponding to reduced viologen (marked with *) can also be seen under S when S is biased negatively.

PEO layers over the S electrode and spectra 5d,e were over the D electrode, for the V_{SG} bias values indicated. Note that if Figure 5a were drawn to scale, the EV/PEO sampled by the Raman beam is closer to the S electrode than to the positive G electrode. It was not possible to observe EV^+ under the G electrode due to its weak Raman scattering. The initial spectra at both the S and D electrode show the 1460 cm^{-1} characteristic peak from neutral PQT (see Figure S2 in Supporting Information), as well as small peaks for the initial EV^{+2} species. With V_{SG} = +2 V, PQT is oxidized and a polaron peak appears at 1405 cm^{-1}. For negative bias with V_{SG} = −2 V, the neutral PQT peak reappears, indicating reduction of polaron back to the neutral state. Under the same bias condition (V_{SG} = −2 V), reduced EV (as EV^+) peaks are also observed over the S electrode (marked with *). This is similar to the EV reduction mechanism as discussed for the two-terminal case in Figure 3 above. For spectra acquired over the D electrode (5d,e), the neutral PQT peak (1460 cm^{-1}) is observed initially, due to the undoped PQT used to fabricate the device. However, the polaron peak is observed over the D terminal with V_{SG} = +2 V, even though the D electrode is floating while V_{SG} is applied. The polaron at both S and D reverts to its neutral state when V_{SG} = −2 V. The EV is partially reduced in the Raman beam because it is close to the negatively biased S (Figure 5c) and reduced PQT. As will be explained below, the two-terminal geometry exhibits opposite oxidation states at S and D under either bias polarity, while in the three-terminal device the oxidation states of *both* the S and D electrodes track the applied bias between the S and G electrodes.

Observation of polarons at both S and D terminals for positive V_{SG} implies that the channel is also filled with polarons. Direct evidence of presence of polarons in the channel is not shown here because the channel gap between the S and D electrodes (1 μm) is smaller than the Raman laser spot size (∼3 μm). To investigate the spatial distribution of polarons in the device, Raman line scans were constructed by acquiring ∼80 spectra along equally spaced points on a line across the gate region, as shown in Figure 6a. The images in Figure 6b−d show the Raman shift along the X axis, the position along Y, and the Raman intensity as false color, with increasing intensity from blue to red. On the as-prepared (initial) device, the Raman peak corresponding to the neutral PQT is prominent along the entire line from S to D sampled by the spectrometer. Intensity in the G region is low compared to that on the S and D terminals due to attenuation of the laser and Raman scattered light by the 30 nm C/Au gate electrode. The main Raman signal intensity from the entire S to D region shifts to the 1405 cm^{-1} position when a SG bias of 2 V is applied, as shown in the Raman image in Figure 6c by the dotted white line. The similar intensities above the D and S electrodes as well as the uniform intensity under the gate between S and D indicates that the conversion of PQT to its polaron has occurred along the entire line between S and D. The oxidation is reversible, with most of the PQT^+ along the SD line reduced back to neutral PQT upon reversal of the bias to V_{SG} = −2 V (Figure 6d). Although each spectrum comprising Figure 6b−d required 10 s to achieve sufficient signal/noise ratio for the image, the peak shift from 1460 to 1405 cm^{-1} occurred as soon as the positive bias was applied. Figure 6c clearly shows the presence of polarons in the device during a +2 V V_{SG}, whereas no signal corresponding to the polaron can be observed in the as-prepared device or during the application of −2 V SG bias.

dx.doi.org/10.1021/ja304458s | J. Am. Chem. Soc. 2012, 134, 14869−14876

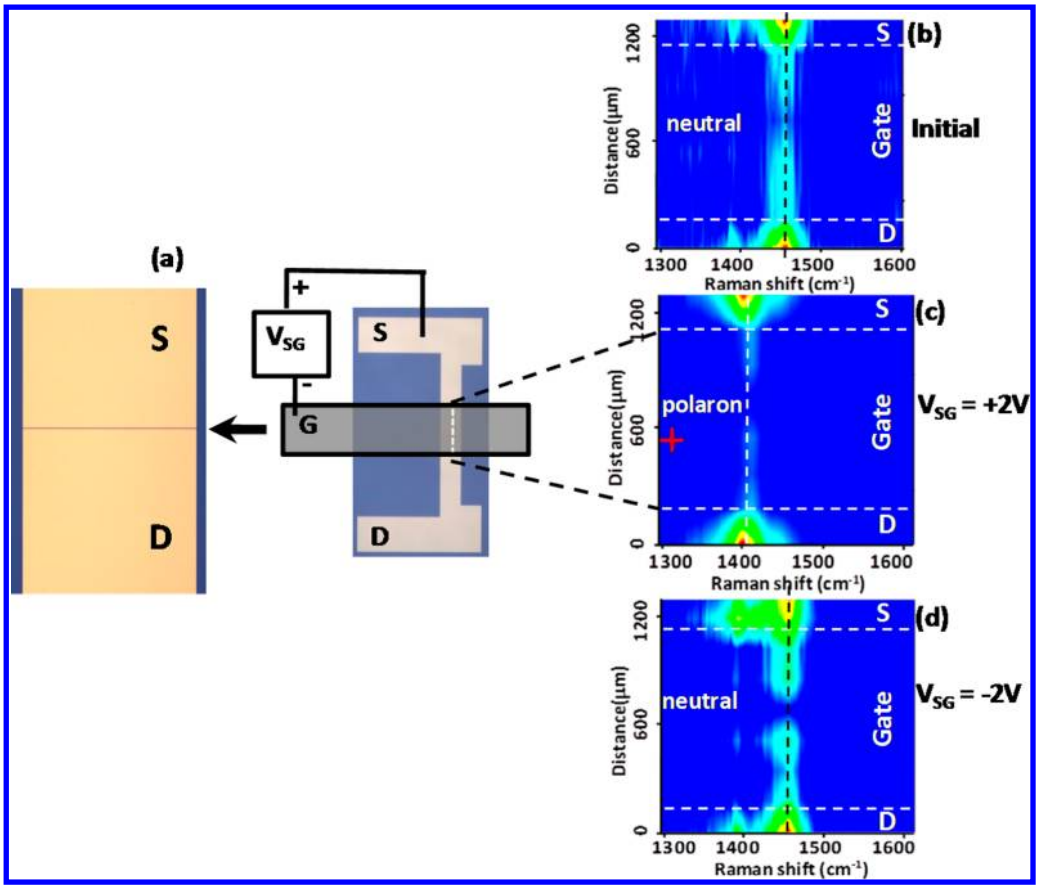

Figure 6. (a) Device schematic with bias polarities. The 1-μm channel is visible as a horizontal line in the left image. (b–d) Raman line scan image from three-terminal devices for the indicated bias values, composed of ten spectra acquired along the line between D and S. Each spectrum was acquired as a sum of fifteen 1-second spectra, and background was subtracted.

It is clear from Raman spectroscopy and microscopy results in Figures 5 and 6 that polarons are formed reversibly at both S and D for appropriate V_{SG} with D floating. Since polarons are more conducting than the neutral state by many orders of magnitude,[24,25] the SD channel conductivity can be switched between high and low values simply by applying appropriate SG bias. These two (low and high) conductivity states can be used as two distinct states of a memory device. It should be noted that the polythiophene bipolaron is also a conductor[26] and possibly present in the high conductivity state, but the Raman evidence supports mainly polaron formation. A schematic of such a device with separate W/E and readout circuits is shown in Figure 7a. Figure 7b shows SD current (I_{SD}) as a function of V_{SD} swept at a rate of 1 V/s before and after V_{SG} pulses of opposite bias, in air. The black curve in Figure 7b was obtained from an as-prepared device in its "initial" state, whereas blue and red curves are obtained after the application of 1-s-long V_{SG} pulses of +2 and −2 V, respectively. Figure 7b clearly shows the increase in SD conductivity after a V_{SG} = +2 V due to formation of conducting polarons in the channel region. The polaron Raman band intensity began to decrease once the VSG bias was removed, as did the channel conductivity. When a V_{SG} = −2 V pulse was applied, the remaining polarons were reduced back to their low conductivity neutral state, resulting in small SD current (red curve). This observation is consistent with the Raman results discussed above and provides a direct correlation of polaron generation from spectroscopy with device conductivity. The oxidation of PQT during the positive

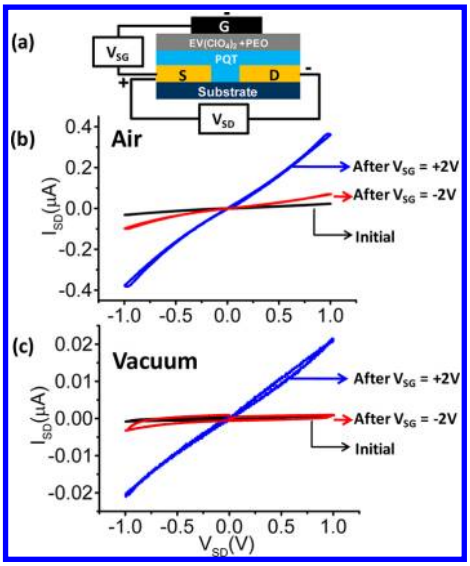

Figure 7. (a) Schematic of a three-terminal memory device. Source–drain I–V (I_{SD}) curves for a three-terminal memory device in its initial state (black), and after a 1 s, +2 V V_{SG} pulse (blue) and 1 s, −2 V V_{SG} pulse in (b) air and (c) vacuum of 10^{-5} Torr for more than 12 h.

(write) pulse is accompanied by the reduction of EV below the G electrode.

We reported previously that trace water can play a role in redox-active junctions by assisting ion transport and/or

dx.doi.org/10.1021/ja304458s | J. Am. Chem. Soc. 2012, 134, 14869–14876

participating in redox reactions.[5,9,11] Raman monitoring of a three-terminal polythiophene (P3HT) device with a silica layer and a Pt gate electrode showed no switching between high and low conductance states after exposure to dry N_2, and it was concluded that water and O_2 were essential to memory operation.[27] To determine if water was important for the memory action of Figure 7b, the experiment was repeated after keeping the sample in a vacuum of $<1 \times 10^{-5}$ Torr for more than 12 h. A memory cycle for the vacuum-dried device is shown in Figure 7c. Although the junction currents are reduced, the switching action remains in a vacuum. The decrease in current occurred within 8-h exposure to vacuum, but no further decrease occurred during 5 days in vacuum thereafter. Therefore, a significant change in the trace water level had minor effects on the polymer redox reactions, presumably because the EV provides the redox counter-reaction and ClO_4^- ion in PEO can migrate to the polymer layer to stabilize the polaron. While PEO is sufficient to permit ion transport in a vacuum, we have noted in related devices that exposure to solvent vapor can significantly promote redox reactions in the solid state.[28]

A faster and more practical alternative to scanning the SD voltage for readout of the memory state is a V_{SD} pulse (0.5 V, 0.5 s), which may be repeated at will to determine the SD conductivity. Figure 8a shows I_{SD} (V_{SD} = 0.5 V) for 0.5 s

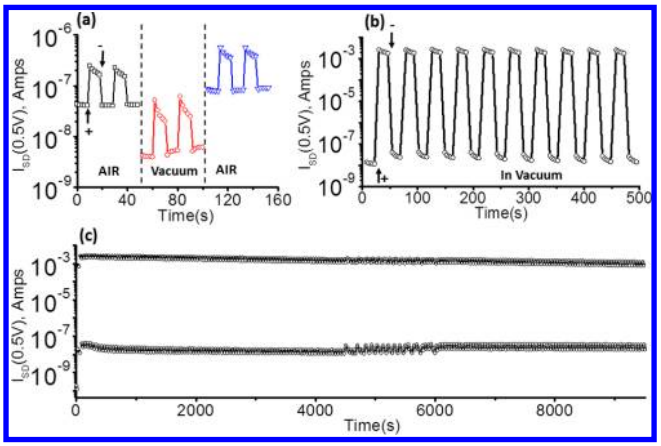

Figure 8. (a) Effect of +2 V and −2 V V_{SG} pulses on subsequent readings at 0.5 V I_{SD} of three-terminal Au/PQT/PEO + $EV(ClO_4)_2$/C/Au devices in air and in vacuum of $<10^{-5}$ Torr, after more than 12 h. The "readout" currents (I_{SD}) were recorded with 0.5 V pulses applied at 2 s intervals. Arrows indicate the application of +2 and −2 V V_{SG}, respectively, of 1 s duration. (b) Ten and (c) 200 W/R/E/R cycles using $V_{SG} = \pm 4$ V, 2 s duration. After each write or erase pulse I_{SD} values were recorded with V_{SD} = 0.5 V at 2 s intervals.

readout pulses in air (black curve), for two W/R/E/R memory cycles monitored by repeated readout pulses before and after +2 V write and −2 V erase pulses applied between the S and G electrodes. Five readings were taken in each state of the device at an interval of 2 s. Figure 8a also shows the result for the same device after 12 h in vacuum (red curve) and then after re-exposure to air (blue curve). Longer sequences of 10 and 200 W/E cycles are shown for another device in parts b and c of Figure 8, respectively, using ±4 V W/E pulses of 2 s duration. Note that the larger switching voltage and time yields an on/offF ratio of $\sim>10^4$, and there is no degradation in this ratio after 10 complete cycles. When a similar device is operated for 100 W/R/E/R cycles in vacuum (2×10^{-6} Torr), there is only a ~10% decrease in the conductance of the ON state, while the on/off ratio remains $>10^4$ (Figure 8c). The origin of the relatively slow changes in the on and off conductance apparent in Figure 8a,b is currently being investigated, but the most likely is a recombination reaction between the PQT^+ polaron and the reduced EV^+ species at their common interface. In a conventional battery, the two redox phases are always separated by an ionic conductor to prevent such recombination, and such a separator is lacking in the current design. We are currently constructing memory devices containing a polyelectrolyte separator layer and a polymeric replacement for EV to reduce or eliminate recombination reactions.

To assess the device yield, three batches of three-terminal devices were made by three different investigators and tested in air with for 10 W/R/E/R cycles, using ±3 V W/E pulses. Sixteen devices on eight chips were tested, all of which showed conductance switching with >100 on/off current ratio. Although the on conductance varied by 1−2 orders of magnitude among these samples, 15 of the 16 had on/off ratios above 10^3, with six of those above 10^4. For six devices chosen randomly on one batch of three chips (two device/chip) made by one investigator, the initial off current was (11 ± 14) nA, the initial on current was (2.1 ± 1.6) mA, and the on/off ratio exceeded 10^4 for all six devices.

The propagation of polaron formation from the S to D electrodes indicated by the spectroscopic results in Figures 5 and 6 is reasonable when the polaron form of the polymer is a conductor. Although the polaron is formed first at the S electrode for a positive V_{SG}, the resulting polaron may undergo redox exchange with adjacent reduced PQT, resulting in propagation of an oxidized "front" of polarons moving away from the S electrode. Since PQT^+ is a conductor, this front may propagate quickly and the S electrode effectively "expands" as the conducting front propagates through the SD gap and onto the D electrode. This moving front is presumably accompanied by transport of ClO_4^- ions into the PQT layer from PEO, to compensate the positive polaron charge. Note that the D electrode may be disconnected externally from the S and G electrodes during propagation, but polarons will still cover D, as shown in Figure 6c. A similar process is operative in electrochromic devices based on conducting polymers, in which oxidation can occur over macroscopic areas. Propagation velocities for such devices have been reported to be 0.1 to >1 mm/s,[29] in which case the time required to oxidize a 1-μm channel is predicted to be less than 1 ms. The erase process may be slower, since the polymer layer adjacent to the S electrode will lose conductivity as the PQT^+ is reduced. The polaron propagation mechanism is shown schematically in Figure 9.

Although the PQT/PEO/EV memory device studied here has the geometry of an organic thin film transistor (TFT), its operation is fundamentally different, involving "electrochemical" rather than "electrostatic" doping of the polythiophene. The current device is analogous to a complete electrochemical battery between the S and G electrodes, with two redox systems and mobile ions to compensate space charge. The reduction of ethyl viologen and associated migration of perchlorate ion provide both an electron acceptor to accompany PQT oxidation and a counterion to stabilize the PQT polaron. However, the three-terminal devices add a third electrode (D), to nondestructively read the conductivity of the polythiophene and to permit independent variation of the SD and SG dimensions and pulse parameters. Thus, the two memory states

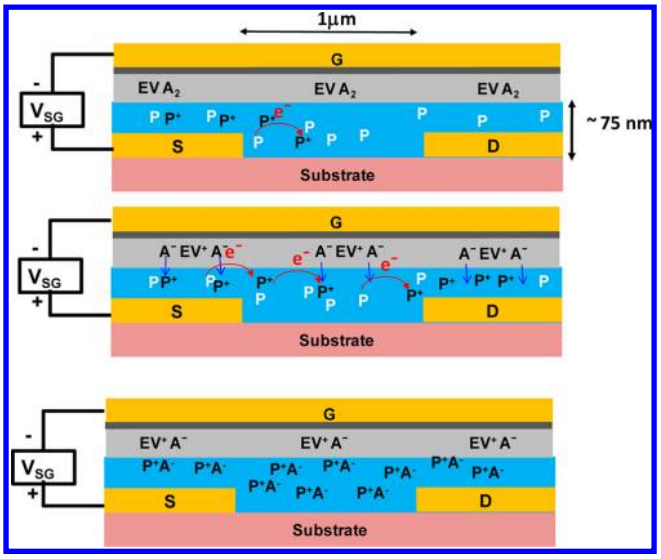

Figure 9. Schematic representation of proposed polaron propagation mechanism, proceeding from top to bottom panels. A^- is perchlorate ion, EV is ethyl viologen, and P is polythiophene. Arrows indicated electron transfers occurring in the polythiophene film. Not drawn to scale.

correspond to the "charged" and "discharged" state of the battery, while the conductance of the SD circuit non-destructively indicates which state is present. As indicated by the voltammetry of both the two-terminal "open face" and three-terminal organic nonvolatile memory (ONVM) devices, the redox reactions ensue when the bias exceeds ~1.2 V, consistent with the thermodynamic redox potentials of PQT^+/PQT and EV^{+2}/EV^+ reactions. As shown in both the point-by-point Raman spectra (Figure 5) and Raman line scans (Figure 6), the conversions between PQT/PQT^+ and EV^{+2}/EV^+ reactions may be monitored with good spatial resolution, although the weak Raman signals dictate relatively slow experiments. Despite this constraint, the spectroscopy provides a definitive description of the switching mechanism and should prove valuable to further device improvements.

The relatively slow write and read speeds of the current ONVM devices is likely due to the time required for heterogeneous electron transfer to the redox agents and the transit time of mobile anions to compensate space charge. These events are not inherently slow, and several changes in composition and design should reduce W/E times to the microsecond to millisecond range and readout to submicroseconds. For example, the transit time for ions may be predicted from the conductivity of solid electrolytes commonly used in solid-state batteries. A solid electrolyte or ionic liquid with a conductivity of 0.001 S/cm at 25 °C (e.g., Nasicon Li^+/Al_2O_3[30]) has a predicted ion transit time across 1 μm at a bias of 1 V of <1 μs. Initial experiments with less ordered polythiophene and alternative electrolytes indicate that ONVM devices with write and erase times in the submillisecond range are quite possible. Given that widely used "flash" memory performs in this speed range, organic devices may become competitive for certain applications. In addition to improving speed, we are also making ONVM devices with ionically conducting separators to improve retention.

CONCLUSIONS

Direct observation of working polythiophene memory devices with spatially resolved Raman spectroscopy permitted direct correlation of conductivity changes with generation of conducting polarons in the polythiophene layer. Propagation of the conducting phase away from the positively biased S electrode results in a high conductivity phase in the channel between S and D as well as throughout the polythiophene film. The viologen/PEO electrolyte provides both a redox counter-reaction to accompany polythiophene oxidation and mobile ions to compensate the positive charge of the conducting polaron. A definitive mechanism for conductance switching provides a rationale for device improvement to achieve faster W/E/R times as well as longer retention and greater cycle life. We will continue to monitor memory operation with Raman and UV–vis spectroscopy, in order to optimize both the composition and design of organic nonvolatile memory.

ASSOCIATED CONTENT

Supporting Information

Reference Raman spectra, spectral changes in devices lacking viologen or polythiophene, various control experiments, and supporting figures and tables. This material is available free of charge via the Internet at http://pubs.acs.org.

AUTHOR INFORMATION

Corresponding Author

mccreery@ualberta.ca

Present Address

[‖]Department of Physics, Indian Institute of Technology, Indore, MP 452017, India.

Notes

The authors declare no competing financial interest.

ACKNOWLEDGMENTS

We acknowledge financial support from the National Institute for Nanotechnology, the Natural Sciences and Engineering Research Council of Canada, Alberta Nanoworks, and the Xerox Research Centre of Canada (XRCC). The authors thank Bryan Szeto for technical assistance with device fabrication.

REFERENCES

(1) Waser, R.; Dittmann, R.; Staikov, G.; Szot, K. *Adv. Mater.* **2009**, *21*, 2632–2663.
(2) Scott, J. C.; Bozano, L. D. *Adv. Mater.* **2007**, *19*, 1452–1463.
(3) Akihito, S. *Mater. Today* **2008**, *11*, 28–36. Linn, E.; Rosezin, R.; Kugeler, C.; Waser, R. *Nat. Mater.* **2010**, *9*, 403–406. Yang, J. J.; Pickett, M. D.; Li, X.; A., O. A.; Stewart, D. R.; Williams, R. S. *Nat. Nanotechnol.* **2008**, *3*, 429–433.
(4) Kwon, D.-H.; Kim, K. M.; Jang, J. H.; Jeon, J. M.; Lee, M. H.; Kim, G. H.; Li, X.-S.; Park, G.-S.; Lee, B.; Han, S.; Kim, M.; Hwang, C. S. *Nat. Nanotechnol.* **2010**, *5*, 148–153. Nauenheim, C.; Kuegeler, C.; Ruediger, A.; Waser, R. *Appl. Phys. Lett.* **2010**, *96*, 122902. Choi, B. J.; Jeong, D. S.; Kim, S. K.; Rohde, C.; Choi, S.; Oh, J. H.; Kim, H. J.; Hwang, C. S.; Szot, K.; Waser, R.; Reichenberg, B.; Tiedke, S. *J. Appl. Phys.* **2005**, *98*, 033715. Liang, C.; Terabe, K.; Hasegawa, T.; Aono, M. *Appl. Phys. Express* **2008**, *1*, 064002.
(5) Shoute, L. C. T.; Pekas, N.; Wu, Y.; McCreery, R. L. *Appl. Phys. A: Mater. Sci. Process.* **2011**, *102*, 841–850.
(6) Barman, S.; Deng, F.; McCreery, R. L. *J. Am. Chem. Soc.* **2008**, *130*, 11073–11081.
(7) Ghosh, B.; Pal, A. J. *J. Phys. Chem. C* **2009**, *113*, 18391–18395.
(8) Zhao, J. H.; Thomson, D. J.; Pillai, R. G.; Freund, M. S. *Appl. Phys. Lett.* **2009**, *94*, 092113. Pillai, R. G.; Zhao, J. H.; Freund, M. S.;

Thomson, D. J. *Adv. Mater.* **2008**, *20*, 49−53. Rahman, G. M. A.; Zhao, J.-H.; Thomson, D. J.; Freund, M. S. *J. Am. Chem. Soc.* **2009**, *131*, 15600−15601.
(9) Wu, J.; McCreery, R. L. *J. Electrochem. Soc.* **2009**, *156*, P29−P37.
(10) Wu, J.; Mobley, K.; McCreery, R. *J. Chem. Phys.* **2007**, *126*, 24704.
(11) Bonifas, A. P.; McCreery, R. L. *Anal. Chem.* **2012**, *84*, 2459−2465.
(12) Bergren, A. J.; McCreery, R. L. *Annu. Rev. Anal. Chem.* **2011**, *4*, 173−195.
(13) Bookbinder, D. C.; Wrighton, M. S. *J. Electrochem. Soc.* **1983**, *130*, 1080−1087. Thackeray, J. W.; White, H. S.; Wrighton, M. S. *J. Phys. Chem.* **1985**, *89*, 5133−5140. Ofer, D.; Crooks, R. M.; Wrighton, M. S. *J. Am. Chem. Soc.* **1990**, *112*, 7869−7879.
(14) Nilsson, D.; Robinson, N.; Berggren, M.; Forchheimer, R. *Adv. Mater.* **2005**, *17*, 353−358.
(15) Ortiz, R. P.; Delgado, M. C. R.; Casado, J.; Hernandez, V.; Kim, O. K.; Woo, H. Y.; Navarrete, J. T. L. *J. Am. Chem. Soc.* **2004**, *126*, 13363−13376. Murphy, A. R.; Frechet, J. M. J.; Chang, P.; Lee, J.; Subramanian, V. *J. Am. Chem. Soc.* **2004**, *126*, 1596−1597.
(16) Ong, B.; Wu, Y.; Jiang, L.; Liu, P.; Murti, K. *Synth. Met.* **2004**, *142*, 49−52.
(17) Wu, Y.; Liu, P.; Ong, B. S.; Srikumar, T.; Zhao, N.; Botton, G.; Zhu, S. *Appl. Phys. Lett.* **2005**, *86*, 142102.
(18) Ong, B. S.; Wu, Y.; Liu, P.; Gardner, S. *J. Am. Chem. Soc.* **2004**, *126*, 3378−3379.
(19) Wu, Y.; Liu, P.; Gardner, S.; Ong, B. S. *Chem. Mater.* **2004**, *17*, 221−223. Bauerle, P.; Fischer, T.; Bidlingmeier, B.; Stabel, A.; Rabe, J. P. *Angew. Chem., Int. Ed.* **1995**, *34*, 303−307.
(20) Mohammad, M. *J. Org. Chem.* **1987**, *52*, 2779−2782. Liu, B.; Blaszczyk, A.; Mayor, M.; Wandlowski, T. *ACS Nano* **2011**, *5*, 5662−5672. Lu, T.; Birke, R. L.; Lombardi, J. R. *Langmuir* **1986**, *2*, 305−309.
(21) Michaelis, L.; Hill, E. S. *J. Gen. Physiol.* **1933**, *16*, 859−873. Han, B.; Li, Z.; Wandlowski, T.; Baszczyk, A.; Mayor, M. *J. Phys. Chem. C* **2007**, *111*, 13855−13863.
(22) Panzer, M. J.; Frisbie, C. D. *J. Am. Chem. Soc.* **2007**, *129*, 6599−6607. Panzer, M. J.; Frisbie, C. D. *J. Am. Chem. Soc.* **2005**, *127*, 6960−6961. Das, A.; Pisana, S.; Chakraborty, B.; Piscanec, S.; Saha, S. K.; Waghmare, U. V.; Novoselov, K. S.; Krishnamurthy, H. R.; Geim, A. K.; Ferrari, A. C.; Sood, A. K. *Nat Nanotechnol.* **2008**, *3*, 210−215. Lu, C.; Fu, Q.; Huang, S.; Liu, J. *Nano Lett.* **2004**, *4*, 623−627. Lee, J.; Kaake, L. G.; Cho, J. H.; Zhu, X.-Y.; Lodge, T. P.; Frisbie, C. D. *J. Phys. Chem. C* **2009**, *113*, 8972−8981. Yuen, J. D.; Dhoot, A. S.; Namdas, E. B.; Coates, N. E.; Heeney, M.; McCulloch, I.; Moses, D.; Heeger, A. J. *J. Am. Chem. Soc.* **2007**, *129*, 14367−14371.
(23) Kumar, R.; Yan, H.; McCreery, R. L.; Bergren, A. J. *Phys. Chem. Chem. Phys.* **2011**, *13*, 14318−14324. Yan, H.; Bergren, A. J.; McCreery, R. L. *J. Am. Chem. Soc.* **2011**, *133*, 19168−19177.
(24) McCullough, R. D.; Lowe, R. D. *J. Chem. Soc., Chem. Commun.* **1992**, 70−72.
(25) McCullough, R. D.; Tristram-Nagle, S.; Williams, S. P.; Lowe, R. D.; Jayaraman, M. *J. Am. Chem. Soc.* **1993**, *115*, 4910−4911. Panzer, M. J.; Frisbie, C. D. *Adv. Funct. Mater.* **2006**, *16*, 1051−1056.
(26) Zotti, G.; Zecchin, S.; Schiavon, G.; Vercelli, B.; Berlin, A.; Dalcanale, E.; Groenendaal, L. B. *Chem. Mater.* **2003**, *15*, 4642−4650. Harima, Y.; Patil, R.; Liu, H.; Ooyama, Y.; Takimiya, K.; Otsubo, T. *J. Phys. Chem. B* **2006**, *110*, 1529−1535.
(27) Shoute,L. C. T.; Wu, Y.; McCreery, R. L. Submitted, 2012
(28) Bonifas, A. P.; McCreery, R. L. *Anal. Chem.* **2012**, *84*, 2459−2465.
(29) Johansson, T.; Persson, N. K.; Inganas, O. *J. Electrochem. Soc.* **2004**, *151*, E119−E124.
(30) Horwat, D.; Billard, A. *Ionics* **2005**, *11*, 120−125. Kudo, T. Survey of types of solid electrolytes. In *CRC Handbook of Solid State Electrochemistry*; Gellings, P. J., Bouwmeester, H. J. M., Eds.; CRC Press, Inc.: New York, 1997; Chapter 6.